

Toward a size scale-up cold sintering process at reduced uniaxial pressure

Sun Hwi Bang¹  | Kosuke Tsuji¹ | Arnaud Ndayishimiye¹  | Sinan Dursun¹ | Joo-Hwan Seo¹ | Stephen Otieno² | Clive A. Randall¹

¹Materials Research Institute and Department of Materials Science and Engineering, Pennsylvania State University, University Park, PA, USA

²Department of Chemistry, Maseno University, Maseno, Kenya

Correspondence

Sun Hwi Bang, Materials Research Institute and Department of Materials Science and Engineering, Pennsylvania State University, University Park, PA, USA.
Email: sbang@psu.edu

Funding information

National Science Foundation, Grant/Award Number: DMR-1728634 and DMR-1756245

Abstract

Cold sintering is a low-temperature powder process methodology that enables the densification of ceramics and ceramic-based composites at significantly reduced times and temperatures. Although the general notion of required pressure for the cold sintering is in the hundreds MPa, some material systems were reasonably demonstrated to be densified in the pressure below 50 MPa, which allows to increase the sample size up to 25 cm² using a small tabletop laboratory press. Indeed, the pressure requirement has been a major constraint on promoting its application deployments, but this study is intended to propose a path to alleviate that limitation. Five different ceramic and composite systems (three ZnO-based composites, Li_{1.5}Al_{0.5}Ge_{1.5}(PO₄)₃, and zeolite Y) with applications in electronic, structural, and energy storage were investigated as a preliminary example of the size scale-up process. One of the observed challenges of the scale-up process was to obtain homogeneous microstructure all over the sample as the transient phase evaporation rate may be different upon the localization. In the case of ZnO, the inhomogeneous pellet translucency may pertain to partial anisotropic grain growth within the same sample.

KEYWORDS

Scale-up process, Low-temperature densification, Cold sintering, Ceramic-Polymer composites, Zinc oxide nanoparticles

1 | INTRODUCTION

Sintering is an established powder processing technique which features the reduction in particle surface area by taking the excess surface free energy as thermodynamic driving force.¹ It has been conventionally recognized that ceramic material sintering process generally requires temperature above 1000°C to reach at least 95% of relative density via atomistic material transport (diffusion), and a quality of dense bulk ceramic is determined by how porosity is effectively removed from the grain structure. However, the early studies on the sintering of materials in the presence of a solvent and uniaxial pressure^{2–4} directed a potential pathway for developing

low-temperature densification process, and hydrothermal hot-pressing method showed that continuous uniaxial compression of a sample under hydrothermal condition resulted powder densification in a close autoclave condition at the sintering temperature below 350°C.⁵

More recently, dense Li₂MoO₄ ceramics were fabricated with moist powder and uniaxial pressure at room temperature.⁶ Then the term, cold sintering process, was coined in 2016 to describe the densification of ceramics and ceramic composites with the presence of transient phase and uniaxial pressure. The significant reduction in the sintering temperature provided a broad perspective of ceramic and polymer process integration.⁷ Several characteristics of the cold sintering revolves around open system

(nonhydrothermal),⁸ short sintering time and low process temperature. Among the reported cold-sinterable material systems, ZnO is often investigated as a model sintering system for its generality. A recent ReaxFF molecular dynamics simulation advanced understanding of mechanism of rapid grain growth kinetics during the cold sintering, showing that the surface hydroxylation can promote Zn cation adsorption on the ZnO surface and hence accelerate recrystallization.⁹

Although there has been rapidly increasing attention on examining new material systems that can be cold sintered, the fundamentals of its sintering mechanisms and kinetics are still in the very early stage of understanding. To date, a geological concept of pressure solution creep can be understood as a governing mechanochemical process that comprehensively explains dissolution, mass transport, and precipitation during the cold sintering.^{10,11} The sintering kinetics can be investigated by classifying four densification process variables including applied uniaxial pressure (P), sintering temperature (T), dwell time (t), and transient chemistry ($\mu(t)$). Correlating the effects of isobaric, isothermal and isochronal conditions to microstructural evolution and specific surface area reduction is an indisputable necessary condition to step forward to advance a complete analytical model of the cold sintering process.

While investigating pressure-dependent sintering kinetics of different materials, we recognized that some systems can be densified even with significantly reduced pressure, which led to curiosity about size scale-up cold sintering process. Indeed, uniaxial pressure in the tens of MPa range can help to develop a vision of industrial implementation for the cold sintering, as the established commercial processes like powder metallurgy consolidation and composite lamination operate within a similar or higher pressure range. Hence, the proposed study is intended to unveil the feasibility of making a large bulk ceramic and ceramic composite at low temperature and pressure for a wide range

of applications including electroceramic, structural, and energy storage materials.

2 | EXPERIMENTAL METHODS

In this study, the scale-up process meant enlarging the size of a cold-sintered specimen from 13-mm diameter to 50-mm length, thus increasing by almost 20 times the sample size that can be produced (Figure 1A,B). The applied uniaxial pressure ranged between 27 and 45 MPa, which is an order of magnitude lower than the general notion of required pressure for the cold sintering. The sintering temperatures of 140–200°C were PID controlled by the temperature readings from the thermocouple inserted at the center of the sintering die, which allows to obtain highly repeatable heating cycles and to compare heating profiles of different sintering die dimensions. The recorded temperature profile showed that the maximum heating rate was 6.1°C/min. and the temperature fluctuation in the steady state was less than 1.0°C (Figure 1C). Multiple thermocouples were inserted to identify any thermal gradient of the sample surface during the process. The densification process variables of the material systems demonstrating the current scale-up study are summarized in Table 1. The envelop density was measured by the Archimedes method using ethanol as a liquid medium, and the sample was soaked in the liquid under vacuum for 30 minutes to completely fill open pores. More details about powder preparation, cold sintering procedures, and materials characterization are documented in the Supplementary Materials.

3 | RESULTS

The photograph of large ZnO showed that partial translucency within the same sample (Figure 2A). It needs to be emphasized

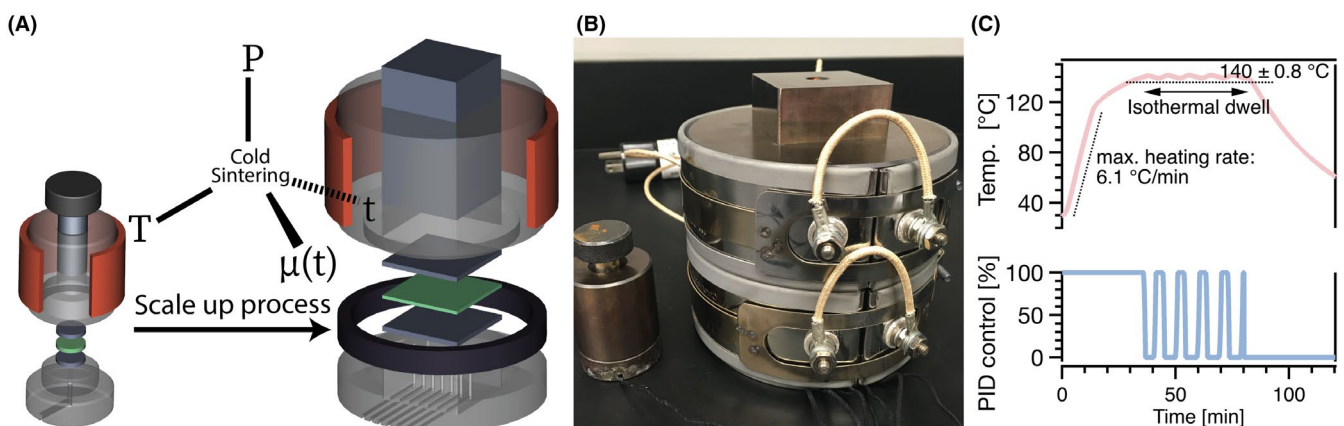


FIGURE 1 (A) Framework illustrating sintering kinetics based scale-up process. (B) Comparison between $\phi = 13$ mm sintering die and $L = 50$ mm. (C) Temperature profile of 140°C and PID control output in a function of time

TABLE 1 Summary of cold-sintered materials where P is the applied uniaxial pressure, T is the sintering temperature, t is the dwell time, and $\mu(t)$ is the transient phase and concentration. C indicates a new cold sintering material system introduced through the current work.

Figure 2	Materials	Ref.	Process conditions			
			P [MPa]	T [°C]	t [min.]	$\mu(t)$
A, F	ZnO	23	27	140	15–480	CH ₃ COOH, 2 M
B, G	ZnO + Aramid nanofibers	C	45	180	0	CH ₃ COOH, 2 M
C, H	ZnO + Polyetherimide + Mn ₂ O ₃ + CoO	C	27	150	60	CH ₃ COOH, 2 M
D, I	Li _{1.5} Al _{0.5} Ge _{1.5} (PO ₄) ₃ (LAGP)	24	27	140	60	DI water
F, J	Zeolite Y	C	27	200	120	NaOH, 5 M

that the thickness of the given sample was 1.06 ± 0.04 mm, which is thicker than typical bulk polycrystalline ceramics regarding the translucency study.¹² Therefore, its interesting optical transmission could be originated from the high degree of densification where the resulting relative density was above 96%. The scanning electron microscope (SEM) micrographs of ZnO identified that the initial spherical particles changed to the faceted grains after cold sintering at 140 °C under uniaxial pressure of 27 MPa (Figure 2F). Comparing the micrographs of isothermal dwell times of 15 and 480 minutes, significant coarsening was observed, where the grain sizes at each isothermal dwell time were 220 ± 76 and 380 ± 170 nm, respectively. Such distinguishable microstructural evolution pertains to (a) Ostwald ripening of precipitated crystals, which are formed by the pressure solution creep process¹³ and (b) accelerated grain coalescence by grain rotation in nano-crystalline precipitates where external stress can enhance the grain rotation rate.¹⁴ However, the size scale-up cold sintering process uses sintering temperature and external pressure that are an order of magnitude lower than the conditions studied in the stress-enhanced

growth simulation.¹⁵ Therefore, it can be conjectured that other factors including the amount of acetate residue phase may be highly relevant to understand fundamental mechanisms of the cold sintering grain growth.

In this study, the scope of ZnO cold sintering was extend to study the feasibility of processing size scale-up ceramic/polymer composite. In the case of the ZnO and aramid nanofiber composite (Figure 2B,H), the relative density was also above 96% and yellowish sample color was originated from the dispersion of aramid nanofiber in the ceramic matrix. Although 0 minute isothermal dwell time was used, the larger grain growth comparing to the pure ZnO at 15 minutes can be relevant to the following factors. (a) The 40°C higher sintering temperature and 18 MPa higher applied uniaxial pressure can provide additional thermodynamic driving force for the enhanced grain growth. (b) Kinetics of the pressure solution creep process will be different with a presence of dimethyl sulfoxide (DMSO), which has a higher evaporation temperature than water.

In the case of the ZnO, polyetherimide, Mn₂O₃, and CoO composite (Figure 2C,H), the relative density was around 88%,

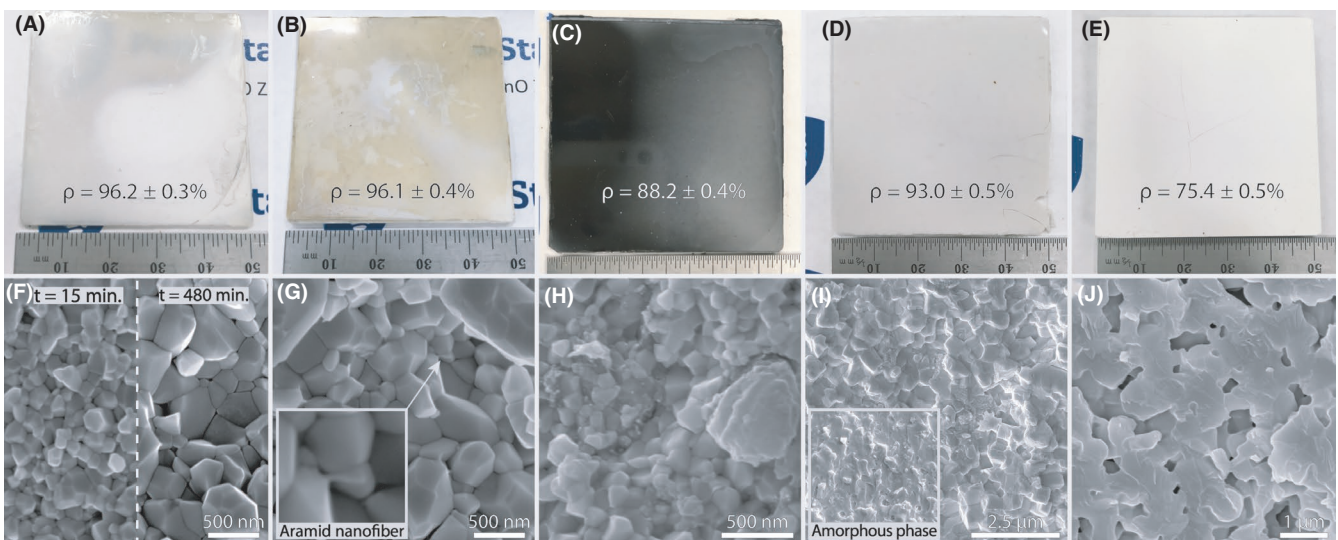


FIGURE 2 Examples of size scaled-up cold-sintered materials. Photographs of (A) ZnO, (B) ZnO + Aramid fiber, (C) ZnO + Polyetherimide + metal oxides, (D) LAGP and (E) Zeolite Y, where ρ indicates the relative density. (F–J) show fractured-surface SEM micrographs of the corresponding materials

which is noticeably lower than that of the first two cases. This can pertain to inhomogeneous mixing between the ceramic particles and the polymer phase, which it can form aggregation and hinder the ceramic phase densification. Hence, obtaining uniform dispersion of polymer and metal oxides, such as using cryogenic grinding, will be necessary to advance understanding on structure-property relationship of multiphase composites.

For the LAGP cold sintering (Figure 2D,I), interparticle neck contact and grain growth were apparent comparing the initial powder and cold-sintered LAGP micrographs (Figure S1A), and high degree of densification was obtained. However, two distinct microstructures of highly crystalline and amorphous regions were both speculated within the same sample. It can be related to inhomogeneous transient phase evaporation during the scale-up cold sintering process, where different degrees of incongruent dissolution can be expected based on local transient phase confinement. Similar to the partial translucency of the pure ZnO cold sintering, enlarging sample size can introduce new complications such as the significantly increases aspect ratio between the surface area and thickness makes the sintered sample prone to crack during the pellet ejection.

Feasibility of zeolite cold sintering was first introduced in this study (Figure 2E,J). Comparing the initial powder and cold-sintered zeolite Y micrographs (Figure S1B), noticeable microstructure change was observed from initial

particle size of 1 μm to neck formation. As shown on the sintered sample micrograph, pore shrinkage was not fully obtained at the given cold sintering conditions, which explains its low density. In fact, dense bulk zeolite Y was previously reported by using hydrothermal sintering process.¹⁶ Although both sintering processes feature reduced processing temperature and applied uniaxial pressure, open system nature of the cold sintering can significantly influence the densification kinetics.¹⁷ Therefore, good understanding of the effect of the densification process variables on the zeolite cold sintering is needed to improve sintering quality at desired microstructure.

4 | DISCUSSION

4.1 | Prospective advantages of the size scale-up cold sintering process

One of the technological advantages of the low-temperature densification is to reduce the temperature processing gap between ceramic and polymer materials, which unlocks new opportunities for investigating functional ceramic-matrix composites with engineered grain boundaries. However, its pressure requirement has been regarded as a

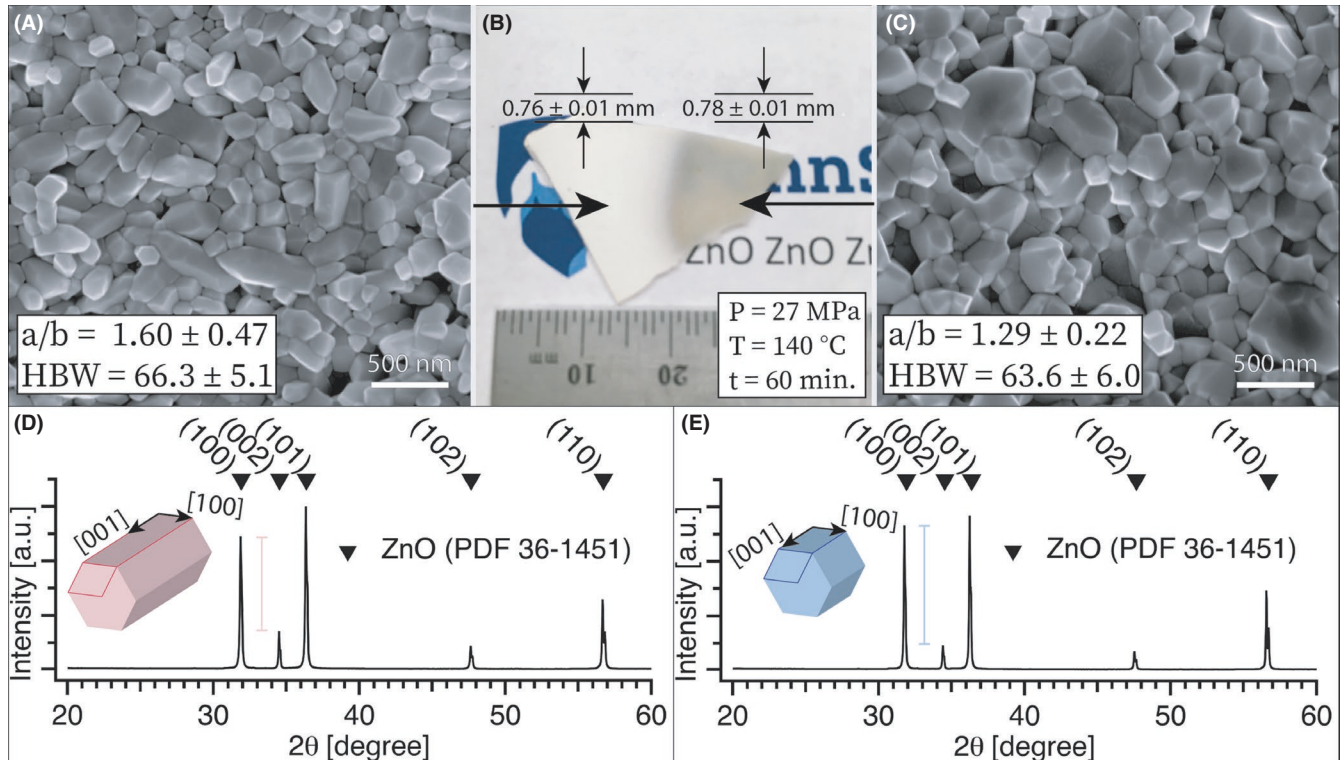


FIGURE 3 Inhomogeneous ZnO translucency. (A) SEM micrograph of the opaque area, where a/b indicates the average grain aspect ratio of 140 grains and HBW corresponds to measured hardness values using the Brinell indentation test. (B) Photograph of the cold-sintered ZnO pellet showing both opaque and translucent part. C, SEM micrograph of the translucent area. XRD patterns of (D) opaque and (E) translucent area, where the bar indicates intensity difference between (001) and (002) peak

major constraint for large-scale manufacturing implementation. The current study observes that the critical pressure for densification may be far lower than the general notion of the cold sintering pressure range, if a target powder and transient chemistry are compatible for initiating the pressure solution creep. More importantly, potential opportunities for the size scale-up is not limited to the field of electroceramic applications including varistor and multilayer capacitor, but includes the research on refractory ceramic matrix with reinforcing aramid nanofiber fillers,¹⁸ molecular sieve adsorbents^{19,20} and all-solid-state batteries.²¹

4.2 | New domain of process challenges

Preliminary observations on the large cold-sintered pellets demonstrate a new domain of process challenges, which needs to be resolved to obtain a uniform microstructure at high density with controlled grain size. In the case of ZnO, both opaque and translucent areas were shown within the same sample (Figure 3A-C), and the locations of those areas were randomly placed, inferring that inhomogeneous pressure distribution is not an appreciable cause. The temperature difference between the center and outer of the sample was measured to be smaller than 1.5°C during the heating ramp, indicating that the temperature gradient can be considered to be minimal. Also, the difference in the sample thickness, Brinell hardness (HBW) and grain size were in the uncertainty range, showing that no significant difference regarding the sintering quality. However, the microstructures identified that the opaque area had more anisotropic grain growth, whereas the translucent area had equiaxed grain evolution. Quantitatively, the average aspect grain ratio of the opaque and translucent regions was 1.60 ± 0.47 and 1.29 ± 0.22 , respectively (Figure S2). The X-ray diffraction (XRD) further qualitatively supported the grain shape difference in the opaque and translucent areas as the peak intensity ratios between (100) and (002) were 0.29 and 0.17, respectively, verifying the anisotropic growth in the [001] direction (Figure 3D,E). Such grain shape results difference in translucency, which pertains to Mie scattering.²² To the our best knowledge, randomly localized transient liquid evaporation rate is a key factor that determines the sample homogeneity.

5 | SUMMARY

We observed that the cold sintering can densify ceramic and ceramic composite materials with the uniaxial pressure below 50 MPa, which is an order of magnitude lower pressure range than the general cold sintering practices. This is an important step in the pathway for its industrial implementation. The use of lower pressure guided to achieve the size scale-up while maintaining


short dwell time and low sintering temperature. However, the enlarged sample size opened a new domain of processing challenges as inhomogeneous grain shape was speculated, which may pertain to randomly localized evaporation of the transient phase. Once the scale-up process is finely tailored to obtain homogeneous sample, thorough investigation is necessary to verify physical properties of each section of the sample. As the development of the cold sintering process is still in the very early stage, it requires lots of advances in fundamental understanding to become a full-fledged powder processing methodology, but this work can be considered as one small step forward.

ACKNOWLEDGMENTS

We sincerely appreciate National Science Foundation (DMR-1728634) for supporting fundamental cold sintering kinetics study. Without the densification kinetics knowledge, the scale-up would not have been possible. We also acknowledge JUAMI, Joint Undertaking for Africa Materials Institute (DMR-1756245) and the program organizing committees, Drs. Simon J. L. Billinge, Sossina M. Haile, and Thomas E. Mallouk for enabling student-driven active research collaboration between U.S. and Africa.

ORCID

Sun Hwi Bang  <https://orcid.org/0000-0001-7492-241X>

Arnaud Ndayishimiye  <https://orcid.org/0000-0003-3853-8239>

REFERENCES

- Mackenzie J, Shuttleworth R. A phenomenological theory of sintering. *Proc Phys Soc B*. 1949;62(12):833–852.
- Roy DM, Gouda G, Bobrowsky A. Very high strength cement pastes prepared by hot pressing and other high pressure techniques. *Cem Concr Res*. 1972;2(3):349–366.
- Hirano S, Somiya S. Hydrothermal reaction sintering of pure Cr₂O₃. *J Am Ceram Soc*. 1976;59(11–12):534–534.
- Yoshimura M, Somiya S. Fabrication of dense, non-stabilized ZrO₂ ceramics by hydrothermal reaction sintering. *Am Ceram Soc Bull*. 1980;59(2):246.
- Yamasaki N, Yanagisawa K, Nishioka M, Kanahara S. A hydrothermal hot-pressing method: apparatus and application. *J Mater Sci letters*. 1986;5(3):355–356.
- Kähäri H, Teirikangas M, Juuti J, Jantunen H. Dielectric properties of lithium molybdate ceramic fabricated at room temperature. *J Am Ceram Soc*. 2014;97(11):3378–3379.
- Guo J, Guo H, Baker AL, Lanagan MT, Kupp ER, Messing GL, et al. Cold sintering: a paradigm shift for processing and integration of ceramics. *Angew Chem Int Ed*. 2016;55(38):11457–11461.
- Goglio G, Ndayishimiye A, Largeteau A, Elissalde C. View point on hydrothermal sintering: main features, today's recent advances and tomorrow's promises. *Scr Mater*. 2019;158:146–152.
- Sengul MY, Guo J, Randall CA, van Duin AC. Water-mediated surface diffusion mechanism enables the cold sintering process: a combined computational and experimental study. *Angew Chem Int Ed*. 2019;58(36):12420–12424.

10. Elliott D. Diffusion flow laws in metamorphic rocks. *Geol Soc Am Bull.* 1973;84(8):2645–2664.
11. Bouville F, Studart AR. Geologically-inspired strong bulk ceramics made with water at room temperature. *Nat Commun.* 2017;8:14655.
12. Bratton R. Translucent sintered MgAl₂O₄. *J Am Ceram Soc.* 1974;57(7):283–286.
13. Sengul MY, Randall CA, Van Duin AC. ReaxFF molecular dynamics simulation of intermolecular structure formation in acetic acid-water mixtures at elevated temperatures and pressures. *J Chem Phys.* 2018;148(16):164506.
14. Chaim R. Grain coalescence by grain rotation in nano-ceramics. *Scrip Mater.* 2012;66(5):269–271.
15. Haslam A, Moldovan D, Yamakov V, Wolf D, Phillpot S, Gleiter H. Stress-enhanced grain growth in a nanocrystalline material by molecular-dynamics simulation. *Acta Mater.* 2003;51(7):2097–2112.
16. Nakahira A, Takezoe S, Yamasaki Y. Synthesis of dense Y-zeolite bulks with large surface area using a hydrothermal hot-pressing (HHP) process. *Chem Lett.* 2004;33(10):1400–1401.
17. Ndayishimiye A, Sengul MY, Bang SH, Tsuji K, Takashima K, de Beauvoir H, et al. Comparing hydrothermal sintering and cold sintering process: mechanisms, microstructure, kinetics and chemistry. *J Eur Ceram Soc.* 2019. <https://doi.org/10.1016/j.jeurceramsoc.2019.11.049>
18. Lin J, Bang SH, Malakooti MH, Sodano HA. Isolation of aramid nanofibers for high strength and toughness polymer nanocomposites. *ACS App Mat Interface.* 2017;9(12):11167–11175.
19. Sachse A, Merceille A, Barrè Y, Grandjean A, Fajula F, Galarneau A. Macroporous LTA-monoliths for in-flow removal of radioactive strontium from aqueous effluents: application to the case of Fukushima. *Microporous Mesoporous Mater.* 2012;164:251–258.
20. Mercier L, Pinnavaia TJ. Heavy metal ion adsorbents formed by the grafting of a thiol functionality to mesoporous silica molecular sieves: factors affecting Hg (II) uptake. *Environ Sci Technol.* 1998;32(18):2749–2754.
21. Li Y, Xu B, Xu H, Duan H, Lü X, Xin S, et al. Hybrid polymer/garnet electrolyte with a small interfacial resistance for lithium-ion batteries. *Angew Chem Int Ed.* 2017;56(3):753–756.
22. Apetz R, Van Bruggen MP. Transparent alumina: a light-scattering model. *J Am Ceram Soc.* 2003;86(3):480–486.
23. Funahashi S, Guo J, Guo H, Wang K, Baker AL, Shiratsuyu K, et al. Demonstration of the cold sintering process study for the densification and grain growth of ZnO ceramics. *J Am Ceram Soc.* 2017;100(2):546–553.
24. Guo J, Berbano SS, Guo H, Baker AL, Lanagan MT, Randall CA. Cold sintering process of composites: bridging the processing temperature gap of ceramic and polymer materials. *Adv Funct Mater.* 2016;26(39):7115–7121.

SUPPORTING INFORMATION

Additional supporting information may be found online in the Supporting Information section.

How to cite this article: Bang SH, Tsuji K, Ndayishimiye A, et al. Toward a size scale-up cold sintering process at reduced uniaxial pressure. *J Am Ceram Soc.* 2020;103:2322–2327. <https://doi.org/10.1111/jace.16976>